MULTIPLE TARGET TRACK-BEFORE-DETECT IN COMPOUND GAUSSIAN CLUTTER

Samuel P. Ebenezer and Antonia Papandreou-Suppappola

School of Electrical, Computer, and Energy Engineering, Arizona State University, Tempe, Arizona 85287
Emails: esamuel@asu.edu and papandreou@asu.edu

ABSTRACT

In this paper, we extend the multiple transition mode track-before-detect (TBD) algorithm to track multiple low observable targets in compound Gaussian sea clutter. The proposed TBD framework uses the un-thresholded fast time radar measurements to track multiple targets in low signal-to-clutter ratios (SCRs). The TBD is implemented using particle filtering (PF), and we derive the generalized likelihood ratio needed to update the particle weights. The maximum likelihood estimate of the texture and the covariance matrix of the speckle are also derived and implemented using a fixed point algorithm. The tracking performance of the proposed algorithm is investigated using three low observable targets that enter and leave the field of view (FOV) at different time steps and under varying environmental conditions.

I. INTRODUCTION

Target tracking in clutter is a challenging problem when the clutter reflected signals have characteristics similar to those of target reflected signals. In moving target indicator applications, the effect of clutter is reduced using Doppler filtering [1]. However, the radial velocity of sea clutter is usually not low due to fast moving waves influenced by weather and wind conditions [2]. Tracking becomes more complicated for multiple low radar cross section (RCS) targets in low signal-to-clutter ratios (SCRs). Recently, track-before-detect (TBD) with particle filtering (PF) has been used to track such low observable targets [3]. A recursive TBD was considered in [4] for estimating clutter statistics as part of the likelihood evaluation step. The clutter was estimated by averaging over a set of nearby bins that are not affected by a target, and a numerical evaluation was used to compute the likelihood ratio for Rayleigh distributed clutter. A multi-scale adaptive single target TBD method was considered in [5], and a Viterbi-like multi-scan TBD algorithm was considered in [6] using complex Gaussian clutter and space-time processing.

Most of the existing TBD algorithms were demonstrated with Gaussian noise and to the best of our knowldedge, we have not come across any multiple target TBD methods that keep track of varying number of targets in low SCR conditions with compound-Gaussian clutter. In this paper, we extend the multiple transition mode multiple target TBD (MMMT-TBD) algorithm we proposed in [7], [8] to track targets in compound Gaussian (CG) sea clutter [2]. Using the CG model, the texture component was assumed to follow a known distribution function in [9], [10]; however, the optimal generalized likelihood function is not mathematically tractable. Various sub-optimal detectors have been considered in [11]–[13]. In [14], the texture component was assumed deterministic. Using this assumption, we derive an optimal likelihood function with the maximum likelihood estimate (MLE) of the texture and the speckle covariance matrix. The MLE can be implemented using an iterative fixed point algorithm [15], [16]. We also analyze the relation between this optimal likelihood function and a sub-optimal one from [11], and we demonstrate the improved tracking performance.

This paper is organized as follows. In Section II, we provide the tracking model needed for the multiple target TBD method. We present the MMMT-TBD method in Section III, and we derive the generalized likelihood function and the MLE of the clutter statistics in Section IV. The proposed algorithm is investigated by tracking three low observable targets in CG clutter under various conditions.

This work was sponsored in part by DARPA under the SSPARC program. The views expressed are those of the authors and do not reflect the official policy or position of the Department of Defense or the U.S. Government.

II. TRACKING MODEL

A. State Model

For the MMMT-TBD method [7], [8], the kinematic state of the targets is estimated, given a maximum possible number of targets $\mathtt{L}$, for M possible target combinations or modes. The posterior probability density function (PDF) of a target is obtained by marginalizing the weighted combination of all possible target combinations in which the target is assumed present.

The dimension of the multi-target state vector $\mathbf{x}_k^i$ depends on the selected mode. For example, if targets two and three are assumed to be present in the ith mode, $i=0,\ldots,M-1$, the multi-target state vector is $\mathbf{x}_k^i=[\mathbf{x}_{k,2}^{\mathsf{T}}\,\mathbf{x}_{k,3}^{\mathsf{T}}]^{\mathsf{T}}$. The state vector of the ℓth target is given by $\mathbf{x}_{k,\ell}=[x_{k,\ell}\;\dot{x}_{k,\ell}\;y_{k,\ell}\;\dot{y}_{k,\ell}]^{\mathsf{T}}$, where $(x_{k,\ell},y_{k,\ell})$ and $(\dot{x}_{k,\ell},\dot{y}_{k,\ell})$ are the two-dimensional (2-D) Cartesian coordinates of the ℓth target position and velocity, respectively, at time step k. The state model for the ℓth target is $\mathbf{x}_{k,\ell}=\mathbf{F}(\mathbf{x}_{k-1,\ell})+\mathbf{v}_{k-1,\ell}$, where $\mathbf{F}$ is a state transition function and $\mathbf{v}_{k-1,\ell}$ is the modeling error.

B. Fast Time Complex Radar Measurement with Clutter

We consider a radar transmitting a dwell of N_p pulses with pulse repetition frequency F_{PRF} Hz. The length of each pulse $s[n]$ is N_s samples. The number of scatterers and their Doppler frequencies are assumed constant during N_p pulses. Using the point source model, the measurement from the pth pulse in a dwell arriving from the ϕth azimuthal direction, $\phi=1,\ldots,N_\phi$, is given by $z_{p,\phi}[n]=\sum_{\ell=1}^{\mathtt{L}_\phi}T_\ell[n]+\sum_{i=1}^{N_r}C_i[n]$, where $T_\ell[n]=\beta_\ell\,s[n-n_\ell]\exp(j2\pi\nu_\ell n)$ is the signal associated with the ℓth target and $C_i[n]=\xi_\phi[i,p]\,s[n-m_{\phi,i}]\exp(j2\pi u_{\phi,i}n)$ is the clutter contribution from the ith range bin, $n=pF_b/F_{\text{PRF}},(pF_b/F_{\text{PRF}})+1,\ldots,((p+1)F_b/F_{\text{PRF}})-1$, F_b Hz is the fast-time sampling frequency, $\mathtt{L}_\phi$ is the number of targets present in the ϕth azimuthal direction, ν_ℓ, n_ℓ and β_ℓ are the Doppler frequency, propagation delay, and complex reflectivity of the ℓth target, respectively, and the corresponding parameters for the ith clutter are $u_{\phi,i}$, $m_{\phi,i}$, and $\xi_\phi[i,p]$.

The overall scatterer contribution at the k dwell is generalized by the $(N_r\times N_p)$ reflectivity matrix $\mathbf{A}_{k,\phi}$. The columns of this

matrix correspond to the reflectivity from all N_p pulses in the kth dwell and the rows represent the reflectivity from $N_r = N_g + N_s - 1$ range bins, where $N_g = \zeta_{k,N_g} - \zeta_{k,1} + 1$ is the number of range bins in the validation gate, and ζ_1 and ζ_{k,N_g} are the first and last range bins in the field of view (FOV). The matrix elements are given by $a_\phi[\zeta_{k,i}, p] = \xi_\phi[\zeta_{k,i}, p] \exp(j2\pi u_{\phi,\zeta_{k,i}} p / F_{\text{PRF}})$. Similarly, a sparse reflectivity matrix corresponding to multiple targets, $\mathbf{T}_{k,\phi}$ can be formulated with non-zero complex reflectivity value in those range bins where a target is present at the kth dwell, in the ϕth azimuthal direction. The range r_k of the target and the corresponding range bin $\zeta_{k,\ell}$ are related by $\zeta_{k,\ell} = \lceil 2r_{k,\ell}/(v_c F_b) \rceil$. The Doppler frequency and the range-rate $\dot{r}_k$ are related by $\nu_\ell = 2\dot{r}_{k,\ell}/(v_c f_c)$, where v_c is the velocity of propagation and f_c Hz is the carrier frequency. A circulant $(N_g \times N_r)$ signal matrix $\mathbf{S}$ is formed from the transmitted signal $s[n]$. The first row of this matrix consists of $s[n]$, followed by $N_r - N_s$ zeros. The remaining rows are generated by circularly shifting this first row to the left. An $(N_g \times N_p)$ measurement matrix can then be written as $\mathbf{Z}_{k,\phi} = \mathbf{S}(\mathbf{T}_{k,\phi} + \mathbf{A}_{k,\phi})$.

The measurements from all azimuthal directions up to the kth dwell are vectorized to represent $\mathbf{z}_k = \text{vec}(\mathbf{Z}_{k,1}, \mathbf{Z}_{k,2}, \ldots, \mathbf{Z}_{k,N_\phi})$ and $\mathbf{Z}_k = \{\mathbf{z}_1, \mathbf{z}_2, \ldots, \mathbf{z}_k\}$ represents all the measurements up to the kth dwell. In order to consider the contribution of the ℓth target, the measurement from range bin $\zeta_{k,\ell}$ in the ϕ_ℓth azimuthal direction is extracted from $\mathbf{Z}_{k,\phi}$ as

$$\mathbf{z}_{k,\phi_\ell}[\zeta_{k,\ell}] = \beta_{k,\ell}\, \mathbf{s}[\nu_\ell] + \mathbf{c}_{k,\phi_\ell}[\zeta_{k,\ell}] \tag{1}$$

where $\mathbf{s}[\nu_\ell] = [1 \ \exp(j2\pi\nu_\ell/F_{\text{PRF}}) \ \ldots \ \exp(j2\pi\nu_\ell(N_p-1)/F_{\text{PRF}})]$, $\beta_{k,\ell}$ is the reflectivity from the target present in range bin $\zeta_{k,\ell}$, and $\mathbf{c}_{k,\phi_\ell}[\zeta_{k,\ell}]$ is the clutter measurement vector corresponding to the $\zeta_{k,\ell}$th row of matrix $\mathbf{S}\mathbf{A}_{k\phi_\ell}$.

C. Compound Gaussian Clutter Model

Signals from high resolution sea-based radars have backscatter due to the presence of gravity waves and sea swells [2]. Using the CG model, small scale components due to multiple scatterers that decorrelate due to relative motion on the sea surface are modeled as speckle. Speckle has a complex Gaussian distribution with a short decorrelation time. It is modulated by a texture component that is slow-varying with longer decorrelation time and associated with long sea waves and swells. Thus, the signal reflectivity is modeled as $\xi_{k,\phi}[\zeta_{k,i}, p] = (\tau_{k,\phi}[\zeta_{k,i}, p])^{1/2}\, x_{k,\phi}[\zeta_{k,i}, p]$, where $\tau_{k,\phi}[\zeta_{k,i}, p] \geq 0$ and $x[\zeta_{k,i}, p]$ represent the texture and speckle components, respectively, for the pth pulse at the kth dwell and in range bin $\zeta_{k,i}$. We assume that the texture is the same for all pulses in a dwell by choosing a very small dwell duration [14]. This is a reasonable assumption due to the slow varying nature of the texture. The clutter from all pulses is given by $\boldsymbol{\xi}_{k,\phi}[\zeta_{k,i}] = [(\tau_{k,\phi}[\zeta_{k,i}])^{1/2}\, x_{k,\phi}[\zeta_{k,i}, 0] \ \ldots \ (\tau_{k,\phi}[\zeta_{k,i}])^{1/2} x_{k,\phi}[\zeta_{k,i}, N_p - 1]]^{\text{T}}$. The speckle is assumed to vary from pulse to pulse. The clutter covariance matrix is given by $\boldsymbol{\Sigma}\, \tau_{k,\phi}[\zeta_{k,i}]$, where $\boldsymbol{\Sigma}$ is the $(N_p \times N_p)$ non-identity complex speckle covariance matrix, which is assumed to be same for all range bins.

D. Doppler Model for Sea Clutter

The small ripples in sea surface are generated by blowing winds that transfer the energy to longer waves. When the wind is blowing at a steady rate, the sea waves reach an equilibrium condition [2]. Clutter from these local wind-driven ripples, that have lower radial velocities, are modeled as Bragg's scattering [17]. These steady state waves are then modulated by sea swells from neighborhood regions under turbulent weather conditions. The radial velocity associated with the modulating sea swells is usually higher than that of the Bragg's scattering. Many empirical studies have shown that the averaged Doppler spectrum of sea clutter can be modeled by a combination of fast non-Bragg scatterers associated with the sea swells and a slow Bragg's scattering associated with smaller capillary waves [18]–[20]. Recently, a linear approximation Doppler spectral model was considered that relates texture and Doppler frequency [21]. Based on this method, we generate the Doppler frequency $\nu^{\text{Bragg}}_{k,\phi}[\zeta_{k,i}]$ of the Bragg's scattering as a normal distribution with mean μ_{Bragg} and variance σ^2_{Bragg}. The sea swell Doppler $\nu^{\text{swell}}_{k,\phi}[\zeta_{k,i}]$ is normally distributed with mean $\mu^{\text{swell}}_{k,\phi}[\zeta_{k,i}] = A_{\text{swell}} + B_{\text{swell}}\, \tau_{k,\phi}[\zeta_{k,i}]$ and variance σ^2_{swell} [21], [22]. The Doppler frequency $u_{\phi,\zeta_{k,i}}$ is randomly selected between the two Doppler frequencies to match real data [18]–[20].

III. MULTIPLE TARGET TBD

When the TBD is used for tracking, the number of detected targets is not assumed to be known *a priori*. In the MMMT-TBD method, the tracking of multiple targets entering and leaving the FOV is formulated as a multiple-model problem as the posterior PDF varies depending on a set of mutually exclusive target combinations or modes. The posterior PDF of the ℓth target is $p(\mathbf{x}_{k,\ell}|\mathbf{Z}_k) = \sum_{i=0}^{M-1} C^i_\ell\, p(\mathbf{x}_{k,l}, m_k = i|\mathbf{Z}_k)$, where C^i_ℓ is a binary indicator that specifies whether target ℓ is present in mode i. The PDF $p(\mathbf{x}_{k,l}, m_k = i|\mathbf{Z}_k)$ is obtained by marginalizing the joint PDF

$$p(\mathbf{x}^i_k, m_k = i|\mathbf{Z}_k) = p(\mathbf{x}^i_k|m_k = i, \mathbf{Z}_k)\ \Pr(m_k = i|\mathbf{Z}_k)$$

for $i = 1, 2, \ldots M-1$. The target state PDF conditioned on a particular mode can be obtained as

$$p(\mathbf{x}^i_k|m_k = i, \mathbf{Z}_k) = \sum_{j=0}^{M-1} p_{j,i}(\mathbf{x}^i_k|\mathbf{Z}_k)\ \Pr(m_{k-1} = j|m_k = i, \mathbf{Z}_k)$$

where $p_{j,i}(\mathbf{x}^i_k|\mathbf{Z}_k) = p(\mathbf{x}^i_k|m_{k-1} = j, m_k = i, \mathbf{Z}_k)$ represents the target state PDF conditioned on transitioning from j at time step $k-1$ to mode i at time step k. Using Bayes rule, the mode conditioned PDF can be written as

$$p_{j,i}(\mathbf{x}^i_k|\mathbf{Z}_k) = L_{j,i}(\mathbf{z}_k|\mathbf{x}^i_k)\ p_{j,i}(\mathbf{x}^i_k|\mathbf{Z}_{k-1}) / L_{j,i}(\mathbf{z}_k|\mathbf{Z}_{k-1}), \tag{2}$$

where $L_{j,i}(\mathbf{z}_k|\mathbf{Z}_{k-1})$ is a normalization factor and $L_{j,i}(\mathbf{z}_k|\mathbf{x}^i_k)$ is the likelihood function conditioned on previous and current modes. The probabilities $\Pr(m_k = i|\mathbf{Z}_k)$ and $\Pr(m_{k-1} = j|m_k = i, \mathbf{Z}_k)$ are derived in [7] based on the likelihood function. The proposed MMMT-TBD was implemented using particle filtering (PF) by approximating the PDFs as $p(\mathbf{x}^i_k|m_{k-1} = j, m_k = i, \mathbf{Z}_k) = \sum_{n=1}^{N_{j,i}} \phi^{(j,i,n)}_k\, \delta(\mathbf{x}^i_k - \mathbf{x}^{(j,i,n)}_k)$, $p(\mathbf{x}^i_k|m_k = i, \mathbf{Z}_k) = \sum_{n=1}^{N_i} \chi^{(i,n)}_k\, \delta(\mathbf{x}^i_k - \mathbf{x}^{(i,n)}_k)$, and $p(\mathbf{x}_{k,\ell}|\mathbf{Z}_k) = \sum_{n=1}^{N_\ell} w^{(n)}_{k,\ell}\, \delta(\mathbf{x}_{k,\ell} - \mathbf{x}^{(n)}_{k,\ell})$. Here, $\phi^{(j,i,n)}_k$, $\chi^{(i,n)}_k$ and $w^{(n)}_{k,\ell}$ are particle weights and $N_{j,i}$, N_i and N_ℓ are number of particles. The generalized likelihood function derived in the next section is used to update the particle weights corresponding to targets entering, surviving or leaving the FOV.

IV. ADAPTIVE LIKELIHOOD FUNCTION

The problem of detecting a target in a range bin can be formulated as the hypothesis problem

$$H_0 : \mathbf{z}_0 = \mathbf{c}_0 \quad H_1 : \mathbf{z}_0 = \beta\mathbf{s} + \mathbf{c}_0 \tag{3}$$

where $\mathbf{c}_0$ is the contribution of clutter to the range bin under test, $\mathbf{s}$ is a known complex signal vector and β is the reflectivity for a target present in this range bin. In this section, for clarity

reasons, vectors $\mathbf{z}_0$ and $\mathbf{s}$ are assumed arbitrary; thus, we ignore the dependence on the target state $\zeta_{k,\ell}$, ν_ℓ, and ϕ_ℓ. Let $\mathbf{z}_0$ represent the measurement from the range bin under test and $\mathbf{z}_i$, $i=1,\ldots,N_T$, are the secondary measurements from N_T neighborhood range bins. The clutter distribution from the (N_T+1) bins are assumed independent and have a complex Gaussian distribution with different power levels. The total speckle power can be included into the texture such that the trace of the speckle covariance matrix is N_p. If the texture is modeled as a random parameter, it is very difficult to jointly maximize the PDF under the H_1 hypothesis, and the closed-form likelihood function does not exist. Various asymptotic detectors were considered in [9], [11]–[13], [23]–[25]. An asymptotically optimum GLRT detector that is invariant to the texture PDF was considered in [11], [13]. The test statistics of this detector in linear quadratic (LQ) form that depends only on the speckle covariance is given by

$$\eta_{\text{LQ}} = |\mathbf{s}^{\text{H}}\boldsymbol{\Sigma}^{-1}\mathbf{z}_0|^2/[(\mathbf{s}^{\text{H}}\boldsymbol{\Sigma}^{-1}\mathbf{s})(\mathbf{z}_0^{\text{H}}\boldsymbol{\Sigma}^{-1}\mathbf{z}_0)]\,. \tag{4}$$

The normalized sample covariance matrix estimate is [12], [26]

$$\hat{\boldsymbol{\Sigma}} = \frac{1}{N_T}\sum_{i=1}^{N_T}(N_p\,\mathbf{z}_i\mathbf{z}_i^{\text{H}})/(\mathbf{z}_i^{\text{H}}\mathbf{z}_i)\,. \tag{5}$$

This estimation is valid only if all the secondary range bins and the range bin under test have the same speckle covariance. We derive a generalized likelihood function (GLR) for the CG clutter using Kelly's approach [27] for a deterministic but time-varying texture. The PDFs of $\mathbf{z}_0$ under H_0 and H_1 are assumed Gaussian with means $\mathbf{0}$ and $\beta\mathbf{s}$ respectively and covariance $\tau_0\boldsymbol{\Sigma}$. Assuming independent clutter, the joint PDF is $p(\mathbf{z}_0,\ldots,\mathbf{z}_{N_T}|H_j) = p(\mathbf{z}_0|H_j)\prod_{i=1}^{N_T}p(\mathbf{z}_i)$, $j=0,1$, where $p(\mathbf{z}_i)$ is Gaussian with mean $\mathbf{0}$ and covariance $\tau_i\boldsymbol{\Sigma}$. The PDF under each hypothesis can be expanded as

$$\begin{aligned} &p(\mathbf{z}_0,\ldots,\mathbf{z}_{N_T}|H_j) \\ &= [\exp(-\text{tr}(\boldsymbol{\Sigma}^{-1}\mathbf{T}_j)/(\pi^{N_p}|\boldsymbol{\Sigma}|\prod_{i=0}^{N_T}\tau_i^{N_p/(N_T+1)})]^{N_T+1} \end{aligned} \tag{6}$$

where

$$\mathbf{T}_0 = \frac{1}{N_T+1}\left(\frac{\mathbf{z}_0\mathbf{z}_0^{\text{H}}}{\tau_0}+\mathbf{S}\right), \mathbf{T}_1 = \frac{1}{N_T+1}\left(\frac{\mathbf{z}_s\mathbf{z}_s^{\text{H}}}{\tau_0}+\mathbf{S}\right) \tag{7}$$

$\mathbf{S}=\sum_{i=1}^{N_T}\mathbf{z}_i\mathbf{z}_i^{\text{H}}/\tau_i$, $\mathbf{z}_s=(\mathbf{z}_0-\beta\mathbf{s})$, and $\text{tr}(\cdot)$, $|\cdot|$ are the trace and determinant of a matrix, respectively.

A. Maximum Likelihood Estimate of Clutter Statistics

In order to obtain the likelihood function, we first need to estimate the clutter statistics $\boldsymbol{\Sigma}$ and τ_i. The MLE of these parameters can be obtained by maximizing the joint PDF over these parameters. If we first assume that the texture is known, the MLE estimate of $\boldsymbol{\Sigma}$ can be obtained by maximizing the log PDF, $\hat{\boldsymbol{\Sigma}}_{\text{MLE}} = [\sum_{i=1}^{N_T}\mathbf{z}_i\mathbf{z}_i^{\text{H}}/\tau_i]/N_T$. If $\boldsymbol{\Sigma}$ is known, the texture MLE can be obtained as $\hat{\tau}_{i,\text{MLE}} = \text{tr}(\boldsymbol{\Sigma}^{-1}\mathbf{z}_i\mathbf{z}_i^{\text{H}})/N_p$, $i=1,\ldots,N_T$. When both the clutter statistics are not known, the above two equations can be solved simultaneously using the iterative fixed point method in [15]. It was shown in [16] that the estimate converges to the true solution, irrespective of the initialization. The converge behavior of the fixed point method are discussed in [15] and [16].

B. Calculation of Generalized Likelihood Function

Using Equations (6) and (7) and the MLE of the parameters, the (N_T+1)th root of the GLR as a function of the unknown target reflectivity and the texture can be written as $L(\tau_0,\beta) = |\mathbf{T}_0|/|\mathbf{T}_1|$, which can be further modified by minimizing the denominator with respect to β. Using steps similar to Kelly's method (CG-K) [27], the GLR can be derived as $L = 1/(1-\eta_{\text{CG-K}})$ where

$$\eta_{\text{CG-K}} = |\mathbf{s}^{\text{H}}\hat{\boldsymbol{\Sigma}}_{\text{MLE}}^{-1}\mathbf{z}_0|^2/(\mathbf{s}^{\text{H}}\hat{\boldsymbol{\Sigma}}_{\text{MLE}}^{-1}\mathbf{s}\,(\hat{\tau}_{0,\text{MLE}}N_T + \mathbf{z}_0^{\text{H}}\hat{\boldsymbol{\Sigma}}_{\text{MLE}}^{-1}\mathbf{z}_0)). \tag{8}$$

The texture for the range bin under test $\hat{\tau}_{0,\text{MLE}}$ cannot be estimated without knowing the target reflectivity. Instead, we can use the estimated texture of the past frame as it changes slowly. The CG-K statistic is related to η_{LQ} in (4) as

$$\eta_{\text{CG-K}} = \eta_{\text{LQ}}\left[\mathbf{z}_0^{\text{H}}\boldsymbol{\Sigma}^{-1}\mathbf{z}_0/(\mathbf{z}_0^{\text{H}}\boldsymbol{\Sigma}^{-1}\mathbf{z}_0+\tau_0 N_T)\right].$$

This suggests that, for a positive definite matrix $\boldsymbol{\Sigma}$, $\eta_{\text{CG-K}}$ is always smaller than η_{LQ}. Under H_0,

$$\eta_{\text{CG-K},H_0} = \eta_{\text{LQ},H_0}[\mathbf{y}_0^{\text{H}}\mathbf{y}_0/(\mathbf{y}_0^{\text{H}}\mathbf{y}_0+N_T)]$$

where $\mathbf{y}_0 = \boldsymbol{\Sigma}^{-1/2}\mathbf{x}_0$ is the whitened version of the speckle component $\mathbf{x}_0$ and $\eta_{\text{CG-K}}$ is invariant to texture under H_0. Under H_1,

$$\eta_{\text{CG-K},H_1} = \eta_{\text{LQ},H_1}\left[\frac{\mathbf{y}_0^{\text{H}}\mathbf{y}_0}{\mathbf{y}_0^{\text{H}}\mathbf{y}_0+N_T}\right]\left[\frac{1+u/(\mathbf{y}_0^{\text{H}}\mathbf{y}_0)}{1+u/(\mathbf{y}_0^{\text{H}}\mathbf{y}_0+N_T)}\right]$$

where $u = \left|\beta(\mathbf{r}^{\text{H}}\mathbf{r}/\tau_0)^{1/2} + \mathbf{y}_0^{\text{H}}\mathbf{r}/(\mathbf{r}^{\text{H}}\mathbf{r})^{1/2}\right|^2 - |\mathbf{y}_0^{\text{H}}\mathbf{r}|^2/(\mathbf{r}^{\text{H}}\mathbf{r})$ and $\mathbf{r} = \boldsymbol{\Sigma}^{-1/2}\mathbf{s}$. For a positive definite matrix $\boldsymbol{\Sigma}$, the scale factor under H_1 is greater than the one under H_0 when one of the following two conditions are satisfied: (i) β is real and positive, and (ii) $|\beta|^2\mathbf{r}^{\text{H}}\mathbf{r} > -2\sqrt{\tau_0}\text{Re}\{\beta\mathbf{y}_0^{\text{H}}\mathbf{r}\}$. The second condition can be satisfied for moderately high SCR. Thus, the variance of $\eta_{\text{CG-K},H_0}$ is smaller than the variance of η_{LQ,H_0}. Under H_1, $\eta_{\text{CG-K},H_1}$ is a scaled version of η_{LQ,H_1}, though the scaling value is smaller than that under H_0. Therefore, the probability of false alarm with CG-K is smaller than with the LQ; the probability of detection is similar for both methods. Hence, the proposed likelihood function is expected to perform better than the sub-optimal method when one of the two conditions is satisfied. Finally, the likelihood function needed for the TBD framework is obtained from the modified binary hypothesis problem in (3) by replacing $\mathbf{z}_0$, $\mathbf{c}_0$, β and $\mathbf{s}$ with $\mathbf{z}_{k,\phi}[\zeta_{k,\ell}]$, $\mathbf{c}_{k,\phi}[\zeta_{k,\ell}]$, $\beta_{k,\ell}$ and $\mathbf{s}[\nu_\ell]$, respectively. For a given target state vector in mode i at the kth dwell, the range and Doppler can be computed as in Section II. The range bin $\zeta_{k,\ell}$ is used to identify $\mathbf{z}_0$ and the Doppler ν_ℓ is used to derive the signal $\mathbf{s}$. The measurement vector model is given in (1), and the GLR is computed using (4) or (8). The likelihood function for the ℓth target can be written as $L(\mathbf{z}_k|\mathbf{x}_{k,\ell}) = 1/[1-\eta(\mathbf{z}_k|\mathbf{x}_{k,\ell})]$. The range of the test statistic $\eta(\cdot)$ is [0 1] [27]. In order to increase the dynamic range of the likelihood function, a likelihood function that varies from zero to infinity is $L(\mathbf{z}_k|\mathbf{x}_{k,\ell}) = \eta(\mathbf{z}_k|\mathbf{x}_{k,\ell})/[1-\eta(\mathbf{z}_k|\mathbf{x}_{k,\ell})]$. This new function is advantageous for use in the multi-target TBD since the joint multi-target PDF is approximated by the product of the likelihood function of each target. If a target is not present, the joint particle weights corresponding to a target mode tend to zero; when all the targets are present, the weights tend to have very high values. This provides better discrimination for particles belonging to various target modes. If the targets are assumed to move independently, the generalized joint likelihood function in (2) is computed as $L_{j,i}(\mathbf{z}_k|\mathbf{x}_k^i) = \prod_{\ell=0}^{\text{L}}(L(\mathbf{z}_k|\mathbf{x}_{k,\ell}^i))^{C_\ell^i}$.

V. SIMULATIONS

The fast time measurement was generated by simulating a high resolution radar with the parameters, $f_c = 10$ GHz, $F_b = 25$ MHz 2 kHz PRF, $N_p = 20$, [15.25 16.75] km validation gate range, $N_g = 249$, 6 m range resolution, 0.703^o beam width, 93.59 m cross-range resolution range, 20 rpm beam scan rate, and $N_\phi = 1$. The clutter signals are synthesized by first generating the matrix

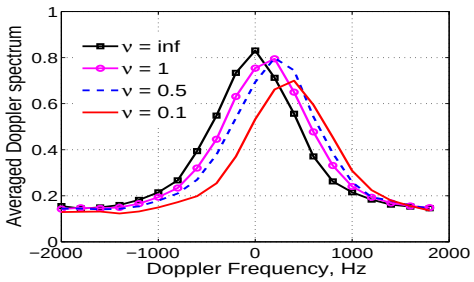

Fig. 1. Averaged Doppler spectrum for different values of c_g.

$\mathbf{A}_{k,\phi}$ in Section IIB. The clutter reflectivity, $\xi_\phi[\zeta_{k,i}, p]$ is generated according to Section IIC. The speckle components $x_{k,\phi}$ are generated from a correlated complex Gaussian distribution and the texture $\tau_{k,\phi}$ was generated from a correlated gamma distribution with scale b_g and shape c_g parameters [2]. The correlation function estimated in [14] using radar measurements collected with the IPIX radar [28] is used. The Doppler model in Section IID is used to generate the Doppler shifts $u_{\phi,\zeta_{k,i}}$. The model parameters are set to $\mu_{\text{Bragg}} = -15$ Hz, $\sigma_{\text{Bragg}} = 7.07$ Hz, $A_{\text{swell}} = 50$ Hz, $B_{\text{swell}} = 5.95$ Hz. The parameter σ_{swell} is sampled from a Gaussian distribution with mean and standard deviation equal to 60 Hz. The spikiness of the texture component is controlled by the shape parameter c_g; decreasing c_g results in more spiky clutter. The averaged Doppler clutter spectrum for different values of c_g is shown in Fig. 1. For higher c_g values, the averaged Doppler spectrum is centered around the assumed Bragg's model parameters, whereas for lower values, the frequency centers around the swell model parameters.

We compared the performance of the algorithm for tracking three targets moving at constant velocity. The targets are assumed to leave and enter the FOV at different time instants (5,25 dwells, 13,33 dwells, 21,41 dwells for targets 1, 2 and 3, respectively). The corresponding initial positions and velocities were (11,312, 11,312) m and (-5.19, -5.18) m/s, (10,959, 10,959) m and (-6.62, -6.63) m/s, (11,666, 11,666) m and (-5.27, -5.26) m/s. All PF in Section III use 500 particles. We compared the performance of the proposed multi-target TBD using the asymptotic detector (LQ) and Kelly's (CG-K) generalized likelihood functions. The effect of using the texture from past frames is also analyzed by comparing the tracking performance with the true and estimated texture components. The LQ method is analyzed using two different covariance estimates: $\hat{\mathbf{\Sigma}}$ in (5) and the MLE assuming the texture component is known.

The tracking error was measured using the OSPA metric with cut-off parameter $c = 500$ and $p = 2$ [29]. The cardinality and the tracking error is combined in the OSPA. The cut-off parameter determines the penalty for missing or detecting a false target and $p = 2$ implies that the Euclidean distance is used to quantify the tracking error. We varied the SCR (3, 0, -3, and -6 dB) and the values of c_g (10, 1, 0.5 and 0.2), and averaged the OSPA values over 200 Monte-Carlo simulations. Figure 2 shows the tracking error for all four cases for varying c_g. The CG-K performs the best for all values of c_g. The CG-K has a similar performance with the estimated and true texture for moderately spiky clutter and the tracking error averages around 30 m. The LQ performs poorly when the clutter is spiky for all covariance matrix estimations. For $c_g = 0.2$, the CG-K tracking performance degraded when using the past frame's texture component, as compared to the true texture component. However, the CG-K with estimated texture components still performed better than LQ. Similarly, Figure 3 shows the tracking error for all four cases for varying SCR. At -6 dB SCR, the LQ method performed better than the other two methods but had more false alarms during time instants 41-46. The performance of the two CG-K based methods was generally better than the two LQ methods at higher SCR. The OSPA metric was higher during target mode transition periods (cardinality error) that happened at dwells 5, 13, 20, 25, 33, and it indicated some delay in detecting a target entering or leaving the FOV.

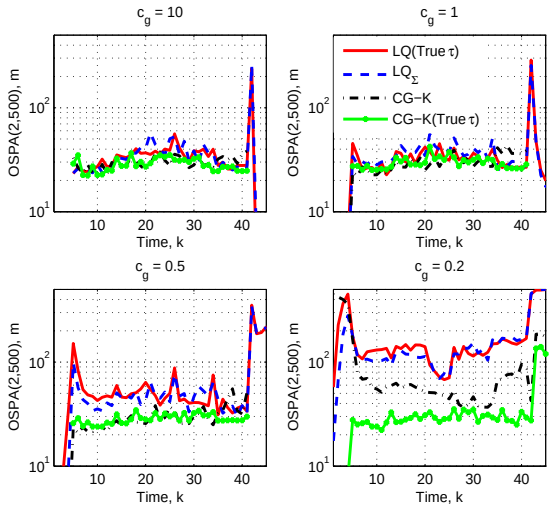

Fig. 2. Tracking error for different values of c_g and 3 dB SCR.

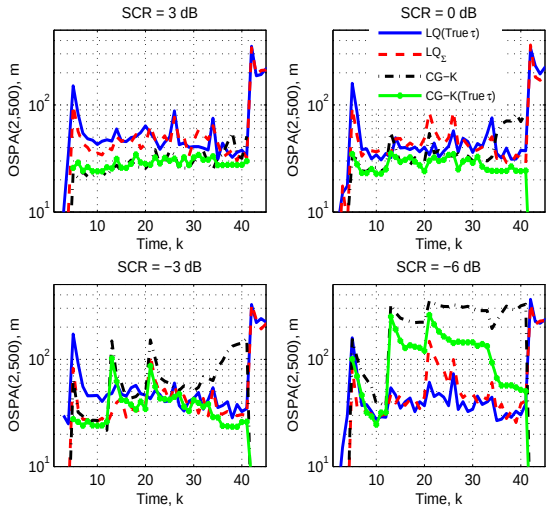

Fig. 3. Tracking error for different values of SCR, $c_g = 0.5$.

VI. CONCLUSION

We derived a generalized likelihood function for multiple targets in compound Gaussian clutter by assuming the texture component to be deterministic and time varying. The MLE of the texture and the speckle covariance matrix were also derived and computed using the fixed point algorithm. The derived likelihood function was used to update the particle weights of a multiple target TBD algorithm. The tracking performance using the proposed likelihood function has improved when compared to using the likelihood function from the classical LQ method.

VII. REFERENCES

[1] M. A. Richards, *Fundamentals of Radar Signal Processing*, McGraw-Hill, New York, 2005.

[2] K. Ward, R. Tough, and S. Watts, *Sea Clutter: Scattering, the K Distribution and Radar Performance*, The Institute of Engineering and Technology, 2 edition, 2013.

[3] B. Ristic, S. Arulampalam, and N. Gordon, *Beyond the Kalman Filter: Particle Filters for Tracking Applications*, Artech House, 2004.

[4] E. Brekke, T. Kirubarajan, and R. Tharmarasa, "Tracking dim targets using integrated clutter estimation," in *Optical Engineering Applications*, 2007, pp. 669905–669905.

[5] M. Farshchian and R. G. Raj, "A multi-scale and adaptive track-before-detect technique for maritime environments," in *IEEE Radar Conference*, May 2011, pp. 818–823.

[6] D. Orlando, L. Venturino, M. Lops, and G. Ricci, "Space-time adaptive algorithms for track-before-detect in clutter environments," in *Int. Radar Conference*, 2009, pp. 1–6.

[7] S. P. Ebenezer and A. Papandreou-Suppappola, "Multiple mode track-before-detect for multiple targets," in *Int. Waveform Design and Diversity Conference*, January 2012.

[8] S. P. Ebenezer and A. Papandreou-Suppappola, "Multiple transition mode multiple target track-before-detect with partitioned sampling," in *IEEE Int. Conference on Acoustics, Speech and Signal Processing*, May 2014, pp. 8008–8012.

[9] P. Stinco, M. Greco, and F. Gini, "Adaptive detection in compound-Gaussian clutter with inverse-gamma texture," in *IEEE CIE International Conference on Radar*, October 2011, vol. 1, pp. 434–437.

[10] A. Balleri, A. Nehorai, and J. Wang, "Maximum likelihood estimation for compound-Gaussian clutter with inverse gamma texture," *IEEE Transactions on Aerospace and Electronic Systems*, vol. 43, no. 2, pp. 775–779, April 2007.

[11] F. Gini and M.V. Greco, "Suboptimum approach to adaptive coherent radar detection in compound-Gaussian clutter," *IEEE Transactions on Aerospace and Electronic Systems*, vol. 35, no. 3, pp. 1095–1104, Jul 1999.

[12] E. Conte, M. Lops, and G. Ricci, "Adaptive detection schemes in compound-Gaussian clutter," *IEEE Transactions on Aerospace and Electronic Systems*, vol. 34, no. 4, pp. 1058–1069, October 1998.

[13] Ernesto Conte, M. Lops, and G. Ricci, "Asymptotically optimum radar detection in compound-Gaussian clutter," *IEEE Transactions on Aerospace and Electronic Systems*, vol. 31, no. 2, pp. 617–625, April 1995.

[14] S.P. Sira, D. Cochran, A. Papandreou-Suppappola, D. Morrell, W. Moran, and S. Howard, "A subspace-based approach to sea clutter suppression for improved target detection," in *Fortieth Asilomar Conference on Signals, Systems and Computers (ACSSC)*, Oct 2006, pp. 752–756.

[15] F. Gini and M. Greco, "Covariance matrix estimation for CFAR detection in correlated heavy tailed clutter," *Signal Processing*, vol. 82, no. 12, pp. 1847–1859, 2002.

[16] F. Pascal, Y. Chitour, J. Ovarlez, P. Forster, and P. Larzabal, "Covariance structure maximum-likelihood estimates in compound Gaussian noise: Existence and algorithm analysis," *IEEE Transactions on Signal Processing*, vol. 56, no. 1, pp. 34–48, January 2008.

[17] M. Skolnik, *Introduction to Radar Systems*, McGraw-Hill, 3 edition, 2001.

[18] I. Antipov, "Statistical analysis of Northern Australian coastline sea clutter data," Tech. Rep. DSTO-TR-1236, Electronics and Surveillance Research Laboratory, Defense Science and Technology Organization, November 2001.

[19] D. Walker, "Doppler modelling of radar sea clutter," *IEE Proceedings of Radar, Sonar and Navigation*, vol. 148, no. 2, pp. 73–80, April 2001.

[20] D. Walker, "Experimentally motivated model for low grazing angle radar Doppler spectra of the sea surface," *IEE Proceedings of Radar, Sonar and Navigation*, vol. 147, no. 3, pp. 114–120, June 2000.

[21] S. Watts, "A new method for the simulation of coherent sea clutter," in *IEEE Radar Conference*, May 2011, pp. 052–057.

[22] S. Watts, "Modeling and simulation of coherent sea clutter," *IEEE Transactions on Aerospace and Electronic Systems*, vol. 48, no. 4, pp. 3303–3317, October 2012.

[23] F. Gini, "Sub-optimum coherent radar detection in a mixture of K-distributed and Gaussian clutter," *IEE Proceedings on Radar, Sonar and Navigation*, vol. 144, pp. 39–48, 1997.

[24] K.J. Sangston, F. Gini, and M.S. Greco, "Coherent radar target detection in heavy-tailed compound-Gaussian clutter," *IEEE Transactions on Aerospace and Electronic Systems*, vol. 48, no. 1, pp. 64–77, Jan 2012.

[25] L. P. Roy and R. V. Rajar Kumar, "A GLRT detector in partially correlated texture based compound-Gaussian clutter," in *National Conference on Communications*, January 2010, pp. 1–5.

[26] Ernesto Conte, Antonio De Maio, and G. Ricci, "Covariance matrix estimation for adaptive CFAR detection in compound-Gaussian clutter," *IEEE Transactions on Aerospace and Electronic Systems*, vol. 38, no. 2, pp. 415–426, Apr 2002.

[27] E. J. Kelly, "An adaptive detection algorithm," *IEEE Transactions on Aerospace and Electronic Systems*, vol. AES-22, pp. 115–127, March 1986.

[28] A Drosopoulos, "Description of the OHGR database," Tech. Rep. 94-14, Defense Research, Ottawa, December 1994.

[29] D. Schuhmacher, Ba-Tuong Vo, and Ba-Ngu Vo, "A consistent metric for performance evaluation of multi-object filters," *IEEE Trans. Signal Processing*, vol. 56, pp. 3447–3457, 2008.